CRYSTAL GROWTH & DESIGN

pubs.acs.org/crystal

Article

Determination of the Na_3AlF_6–Y_2O_3 Phase Diagram and Its Implications for Low-Temperature YAG/Nd:YAG Synthesis

Michal Korenko,* František Šimko,* Mathieu Allix, Aydar Rakhmatullin, Michael J. Pitcher, and Graham King

Cite This: *Cryst. Growth Des.* 2024, 24, 7494–7503

Read Online

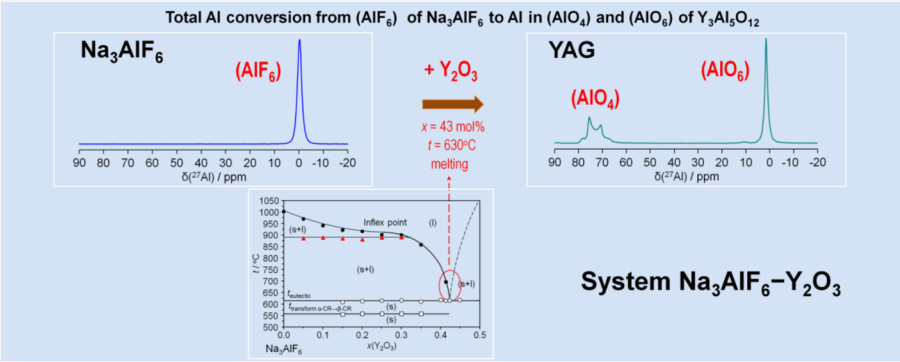

ABSTRACT: A new way of preparing YAG, $Y_3Al_5O_{12}$, materials at low temperatures has been discovered using a molten Na_3AlF_6–Y_2O_3 reaction mixture. For the successful synthesis of YAG, a precise examination of the cryolite part of the phase diagram of the Na_3AlF_6–Y_2O_3 system was carried out up to 45 mol % of Y_2O_3 using thermal analysis with a larger amount of sample (12 g). The phase diagram of the Na_3AlF_6–Y_2O_3 system was discovered to be likely a simple eutectic system with one inflection point on the liquidus curve (coordinates: 22.0 mol % Y_2O_3, 920 °C) and one eutectic point (coordinates: 43.0 mol % Y_2O_3, 620 °C). The spontaneously solidified samples of Na_3AlF_6–Y_2O_3 after thermal analysis have been investigated using solid-state NMR (^{19}F, ^{23}Na, and ^{27}Al) spectroscopy and X-ray powder diffraction over a broad range of compositions. The minimal synthesis temperature used in this work for the preparation of YAG was 630 °C, and the Y_2O_3 concentration was 43 mol %. Besides the synthesis of YAG, the molten Na_3AlF_6–Y_2O_3 system with the addition of Nd_2O_3 has been successfully used also for the preparation of the neodymium-doped YAG powders (Nd:YAG). Rietveld refinement has been used to quantitatively assess the incorporation of neodymium into YAG and β-$Na(Y_{1.5}Na_{0.5})F_6$ materials.

■ INTRODUCTION

Yttrium aluminum garnet $Y_3Al_5O_{12}$ (YAG) is a widely used material that has significant commercial and technological applications in white light-emitting diode (LED) lighting,[1] solid-state lasers,[2] and scintillation detectors.[3] YAG structure with the unit the cell parameter 12.0089 Å consists of three Y^{3+} cations per formula unit exclusively in 8-fold dodecahedral coordination by oxide at the A site (YO_8), with five Al^{3+} cations distributed between the octahedral B site (AlO_6) and tetrahedral C site (AlO_4). This offers chemical flexibility as the A (Y^{3+}) site is able to accommodate most of the rare-earth element (REE^{3+}) dopants, whereas the B and C (Al^{3+}) sites can be replaced with other transition- and post-transition metals, resulting in a number of characteristic emission bands of this garnet material that potentiate its practical use. Besides the above-mentioned characteristics of YAG, chemical and thermal stability, mechanical strength, and other optical characteristics are the main practical advantages of this material.[4]

The conventional method for synthesizing YAG is high-temperature solid-state reaction using oxide raw materials. The initial raw materials must be mixed homogeneously before synthesis and sintered at high temperature (>1600 °C) to produce a single YAG phase without the two coexisting yet not desirable intermediate phases, $YAlO_3$ (yttrium aluminum perovskite, YAP) and $Y_4Al_2O_9$ (yttrium aluminum monoclinic, YAM).[5] As a result, time- and energy-intensive crushing and grinding processes are required to get the desired particle size of the powders prior to further operation.[6,7] Unfortunately, these extra procedures can introduce impurities and defects,

Received: May 21, 2024
Revised: September 3, 2024
Accepted: September 3, 2024
Published: September 9, 2024

resulting in a possibly final significant decrease in the YAG emission efficiency.

Inorganic molten salts as high-temperature ionic liquids have various beneficial physicochemical qualities as solvents and reaction media, including a higher oxidizing potential, high mass transfer, high heat and electrical conductivity, and significantly lower viscosities, densities, and vapor pressure. Thus, when compared to conventional solid-state reactions (or high-temperature reactions from molten oxides), molten salt synthesis is one of the simplest methods for fast, cost-effective, and low-temperature ways for obtaining crystalline, chemically relatively pure oxide/nonoxide powders.

It has been demonstrated that molten salt synthesis can reduce the synthesis temperature more efficiently than the typical solid-state reaction approach. Another important and preferential factor is that low-temperature, solution−based synthesis below 1000 °C can help stabilize newly discovered, highly nonstoichiometric forms of YAGs,[8] as well as new, unusually metastable doped YAGs.[9]

To synthesize YAG powders at lower temperatures, several wet chemical synthesis methods such as sol−gel,[6] coprecipitation,[7,10] spray pyrolysis,[11] and solvothermal[12] have been developed in recent years. However, these approaches still have drawbacks, such as expensive equipment, difficult synthesis procedures, and environmentally hazardous precursors and solvents. Molten salt synthesis is a relatively recent synthesis approach that has been successfully used in synthesizing various ceramic powders and phosphors, including Eu^{3+} doped Y_2O_3 and Lu_2O_3.[13−17]

Yang et al.[18] and Wu et al.[19] reported molten salt synthesis of Ce:YAG phosphor employing Y, Ce, and Al nitrate hydrates or chloride hydrates as starting materials, calcined at 1100 °C. Lin et al.[4] reported using molten chlorides and nanosized oxide particles to synthesize YAG nanopowders. Nevertheless, hazardous gases such as nitrogen oxides or hydrogen chloride may be formed during the process of heating, especially when using molten nitrate hydrates or molten chloride hydrates. Therefore, it is still necessary to investigate new molten salt approaches for the synthesis of YAG at low temperatures.

To the best of our knowledge, there are no publications on the preparation of YAG or other functional materials using the molten fluoride synthesis method. The utilization of molten fluorides for oxides synthesis has one advantage over widely used molten chlorides and other molten salts:[17] molten fluorides, notably sodium cryolite, are very good solvents of oxides (e.g., Al_2O_3, SiO_2, MgO, La_2O_3, Ce_2O_3, etc.).[20,21] Sodium cryolite, sodium hexafluoroaluminate (Na_3AlF_6), is the complex species present in the binary system of NaF and AlF_3 at a molar ratio of 1:3. Sodium cryolite is the most famous fluoroaluminate highly reactive agent used in industrial molten salt chemistry. Its best-known application is the use as an electrolyte for the industrial production of primary aluminum from Al_2O_3 in the so-called Hall−Héroult process.[20]

The usefulness of a simple molten fluoride synthesis process based on molten cryolite for the preparation of YAG ($Y_3Al_5O_{12}$) and Nd-doped YAG (Nd:YAG) was investigated in this study. For the first time, it has been demonstrated that crystallized YAG and Nd-doped YAG may be produced without the use of any alumina at temperatures as low as 630 °C (compared to 1600 °C of the solid-state conversion) utilizing only the molten cryolite (Na_3AlF_6)−yttria (Y_2O_3) reaction mixture where cryolite works as a solvent and source of Al and yttria as a solute and source of Y and O. The possible mechanism of the YAG synthesis is also addressed. Another valuable piece of information presented and published for the first time in this work is the experimental determination of the cryolite-rich part of the phase diagram of the Na_3AlF_6−Y_2O_3 system. Although molten cryolitic systems are one of the most studied molten salt systems with a lot of phase equilibrium data collected in the literature,[21] there is no information available specifically about the solubility of yttria in molten cryolite. With no literature data about the phase equilibria in the Na_3AlF_6−Y_2O_3 system, the first objective prior to the synthesis of YAG itself was to find out the solubility of Y_2O_3 in molten cryolite as the possible reactant for the preparation of YAG. It will be shown that the molten fluoride synthesis procedure using molten Na_3AlF_6 could be a feasible way for the synthesis of YAG and potentially other oxide materials.

■ EXPERIMENTAL SECTION

Materials and Chemicals Used in Experiments. For the preparation of the samples, the following chemicals were used: sodium fluoride (NaF, CAS number: 7681-49-4, Sigma−Aldrich, 99.9%, Germany), aluminum fluoride (AlF_3, CAS number: 7784-18-1, resublimated and dried at 300 °C for min. 4 h, Slovalco, 99.0%, Slovakia), yttrium oxide (Y_2O_3, CAS number: 1314-36-9, Sigma-Aldrich, 99.99%, Germany), and neodymium oxide (Nd_2O_3, CAS number: 1313-97-9, Sigma-Aldrich, 99.9%, Germany). All chemicals were stored in a glovebox under an argon atmosphere (Ar, CAS number: 7440-37-1, Siad, 99.999%, Slovakia) and maintained below 0.3 ppm of moisture and 0.1−0.5 ppm of oxygen.

Thermal Analysis Measurements and Preparation of Chemicals. The phase equilibria of the examined system were determined by using a thermal analysis method. All samples were prepared in a glovebox with an inert argon environment (Ar, 99.999%, SIAD, Slovakia). The 12 g powdered samples were homogenized in an inert environment before being transported in a platinum crucible to a preheated (about 90 °C) electric resistance furnace with a dry argon atmosphere (99.999%, SIAD, Slovakia). One platinum crucible holds the sample, while the other contains the reference material (high-purity Al_2O_3 powders). The temperature of the furnace was controlled by a Pt10Rh/Pt thermocouple put into the reference material. The furnace was, at the beginning, heated at a rate of 7 °C/min to a temperature of 50 °C higher than the melting point of the investigated mixture. The samples were then maintained at this temperature for around 50 min. The temperature of primary crystallization and other heat effects were measured and recorded at a cooling rate of 1.4 °C/min. Such a slow cooling rate is critical for molten systems that tend to undercool. A larger amount of samples (12 g) and a higher bulk-to-surface ratio improve the sensitivity of enthalpic change detection and minimize the influence of evaporation of the measured systems. A computerized measuring instrument (multicomponent model for thermal analysis data collections, National Instruments where the data collections run online under Labview software environment) built at the Institute of Inorganic Chemistry SAS, Slovakia, was used to regulate the furnace's temperature and collect data. The sample's temperature was controlled using a Pt10Rh/Pt thermocouple validated based on the known melting points of the following pure chemicals: NaCl, NaF, and Li_2CO_3. The accuracy of the temperature measurement of the measured thermocouples was found to be ±2 °C. More details about the method can be found elsewhere.[22]

Analysis of the Solidified Samples after Thermal Analysis and the Preparation of the Synthesis Experiments. The solidified samples, after thermal analysis, were moved to a glovebox, homogenized, and analyzed by XRD analysis and solid-state NMR. Also, the samples for the synthesis experiments (reaction mixtures) were prepared in the glovebox in the platinum crucible covered with a lid before being transferred to the resistance furnace and heated to the appropriate synthesis temperature. Some synthesis experiments were also performed in the air. Different reaction durations and

https://doi.org/10.1021/acs.cgd.4c00684
Cryst. Growth Des. 2024, 24, 7494−7503

temperatures were used for the synthesis experiments. All mixtures were then spontaneously cooled to 100 °C, quickly moved to a glovebox, homogenized, and analyzed by XRD analysis and/or by solid-state NMR.

X-ray Diffraction Analysis. X-ray powder diffraction (XRD) patterns of spontaneously cooled samples were measured using an Empyrean PANalytical diffractometer with Cu $K_{\alpha 1,2}$ radiation in Bragg−Brentano geometry and a β filter (Ni). A solid-state PIXcel detector was utilized to record the XRD patterns. The measurements were taken at room temperature, with 2θ ranging from 5 to 80° with a step of 0.016°. Phase analysis was carried out using Oxford Cryosystem Crystallographica Search−Match 2.1 software and the PDF2 2011 database.

Solid-State NMR Analysis. All NMR measurements were performed using a Bruker Avance NEO 850 (20 T) NMR spectrometer. ^{27}Al, ^{23}Na, and ^{19}F spectra were acquired using 1.3 mm diameter rotors at a rotor frequency of 60 kHz. The measured chemical shifts are referenced to $CFCl_3$, 0.1 M NaCl, and $Al(NO_3)_3$ for ^{19}F, ^{23}Na, and ^{27}Al, respectively. The NMR parameters (chemical shifts, line widths, and quadrupolar coupling parameters) were fitted to the observed spectra employing the DMfit2023 program.[23]

■ RESULTS

The initial limitation to using molten cryolite for YAG synthesis was a lack of knowledge regarding the solubility of yttria in such a molten environment. We initially planned to use cryolite's capacity to dissolve alumina and other oxides. With no literature data, the first goal was to determine the phase diagram of the Na_3AlF_6−Y_2O_3 system. The thermal analysis was used to achieve this goal.

Phase Equilibria of the Na_3AlF_6−Y_2O_3 System. The results of the thermal analysis experiment on the investigated system Na_3AlF_6−Y_2O_3 up to 45 mol % of Y_2O_3 are shown in Figure 1. The phase diagram depicted in this picture was

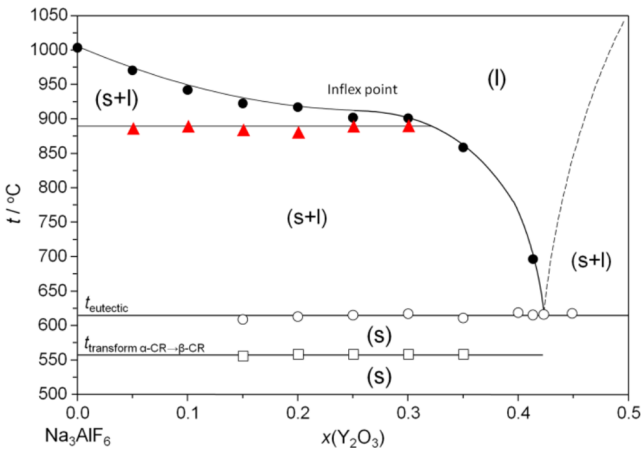

Figure 1. Cryolite-rich part of the phase diagram of the system Na_3AlF_6−Y_2O_3. Full circles: temperatures of primary crystallizations; triangles: temperatures of the second heat effect, which divide two different phase fields of the coexistence of the solid and liquid phases; open circles: eutectic line; open squares: temperature of the α and β cryolite solid−solid transformation; black lines: formal lines, dashed line: expected Y_2O_3 solidus line.

constructed based on the information on the temperatures of the related heat effects obtained on the particular cooling curves acquired during the thermal analysis measurement. The Na_3AlF_6−Y_2O_3 system was discovered to be a simple eutectic system with one eutectic point, E_1, and one inflection point on the liquidus curve, I_1. The system also presents a solid−solid transformation between α and β forms of Na_3AlF_6, T_1. The coordinates of these phase equilibrium characteristics are as followsI_1: 22.0 mol % Y_2O_3, 78.0 mol % CR, $t(I_1)$ = 920 °C,

E_1: 43.0 mol % Y_2O_3, 57.0 mol % CR, $t(E_1)$ = 620 °C,

T_1: solid−solid phase transitions of α and β form of Na_3AlF_6, $t(T_1)$ = 560 °C.

Figure 2 shows the results of the room temperature X-ray diffraction analysis of the investigated spontaneously solidified

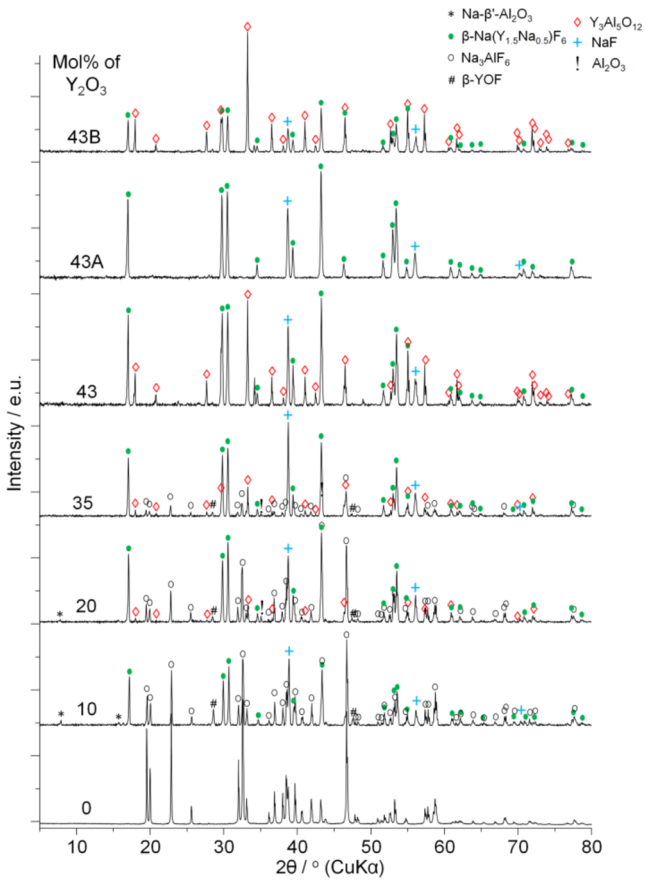

Figure 2. XRD patterns of the spontaneously solidified samples of the Na_3AlF_6−Y_2O_3 system taken after the thermal analysis as a function of Y_2O_3 concentration. 43A: the softer part of the sample, 43B: the harder part of the sample, and 43: XRD pattern of the related sample when both parts were analyzed together.

samples performed after thermal analysis measurement. The results of the XRD analysis can be divided into two groups: the results of the samples with the concentration up to the inflection point (22.0 mol % of Y_2O_3) and the results of the samples with higher concentrations. The presence of the following species was detected in the samples in the first group (concentration up to the inflection point).

Na_3AlF_6 (decreasing intensity of reflections with increasing concentration of Y_2O_3),

NaF (increasing intensity of reflections with the increasing content of Y_2O_3),

β−$Na(Y_{1.5}Na_{0.5})F_6$ (increasing intensity of reflections with the increasing content of Y_2O_3),

β−YOF (relatively constant intensity of reflections vs concentration of Y_2O_3),

$NaAl_{11}O_{17}$ (relatively constant intensity of reflections vs concentration of Y_2O_3),

https://doi.org/10.1021/acs.cgd.4c00684
Cryst. Growth Des. 2024, 24, 7494−7503

YAG, $Y_3Al_5O_{12}$ (first detection of YAG in the sample with 20 mol % concentration of the Y_2O_3).

With the increasing concentration of Y_2O_3 in the samples (beyond the inflection point, i.e., >22.0 mol % of Y_2O_3), the following patterns have been identified (Figure 2).

Na_3AlF_6 (decreasing intensity of reflections with the increasing concentration of Y_2O_3, no reflection of Na_3AlF_6 in the sample for the eutectic composition),

NaF (relatively constant intensity of reflections vs concentration of Y_2O_3),

β−$Na(Y_{1.5}Na_{0.5})F_6$ (relatively constant intensity of reflections vs concentration of Y_2O_3),

β−YOF (decreasing intensity of reflections with the increasing concentration of Y_2O_3, no reflection of β−YOF in the sample for the eutectic composition),

YAG, $Y_3Al_5O_{12}$ (increase of reflections with the increasing concentration of Y_2O_3).

Figure 2 also shows the results of the room temperature X-ray diffraction analysis of the spontaneously solidified sample after thermal analysis with eutectic composition (43, 43A, 43B). The solidified sample had at first sight two separable parts: a harder lower part (43B) and a softer upper part (43A). The softer part contains only reflections of β-$Na(Y_{1.5}Na_{0.5})F_6$ and NaF. The harder part contains, on the other hand, the dominant reflections of YAG and β-$Na(Y_{1.5}Na_{0.5})F_6$ and smaller reflections of NaF.

The relatively unusual shape (with the inflection point) of the liquidus curve of the cryolite in the phase diagram of Na_3AlF_6−Y_2O_3 (Figure 1) can be in some way interrelated with the formation of YAG. The intensity of the reflections of Na_3AlF_6 continually decreases with the increasing concentration of Y_2O_3 in the samples until the eutectic point where Na_3AlF_6 completely disappears. The intensity of reflections of YOF is, on the other hand, relatively constant in the whole spectrum of concentration of Y_2O_3 between 5 and 35 mol %, with complete disappearance at the concentration of the eutectic point (43 mol %). The above-mentioned observation suggests that the formation of β-YOF may, in this system, act as an intermediate step in the production of YAG. When the content of Y_2O_3 reaches the critical concentration in the system (inflection point), β−YOF may start to work as a precursor for the formation of YAG.

Figures 3 and 4 show solid-state ^{27}Al, ^{23}Na, and ^{19}F NMR spectra of the spontaneously solidified samples after thermal analysis measurements (in the concentration range of 10−43 mol % of Y_2O_3). The assignment of resonances was made based on the following references and reflections: YAG (^{27}Al),[24] β'-Al_2O_3 (^{27}Al),[25] YOF,[26,27] and β-$Na(Y_{1.5}Na_{0.5})F_6$.[28] A significant overlap between the ^{23}Na signals of eight coordination environment Na_3AlF_6 and both nine coordinated sodium sites of β-$Na(Y_{1.5}Na_{0.5})F_6$ can be seen in Figure 3 (chemical shift between −5 and −10 ppm). However, at 43 mol % of Y_2O_3, the presence of cryolite disappeared, so we can assign the signals between −5 and −10 ppm also to β-$Na(Y_{1.5}Na_{0.5})F_6$.

NMR analysis confirms the XRD results. The first signals of YAG appeared in the sample with 20 mol % of Y_2O_3 (inflection point in the phase diagram, Figure 1) and became more pronounced in the samples with higher concentrations of Y_2O_3. α-Al_2O_3 appeared in the samples up to 35 mol % of Y_2O_3, and β'-Al_2O_3 was found only in the sample with the lowest concentration of Y_2O_3 (10 mol %). β-$Na(Y_{1.5}Na_{0.5})F_6$, NaF, β-YOF, and Na_3AlF_6 were identified in all investigated samples. The intensity of the α-Al_2O_3 peaks increases until the concentration related to the inflection point (20 mol %) and then decreases and completely disappears in the sample with the highest concentration of Y_2O_3. In the sample with the highest concentration of Y_2O_3, besides dominant signals of YAG, β-$Na(Y_{1.5}Na_{0.5})F_6$, and NaF, only small signals of Na_3AlF_6 and β-YOF appeared.

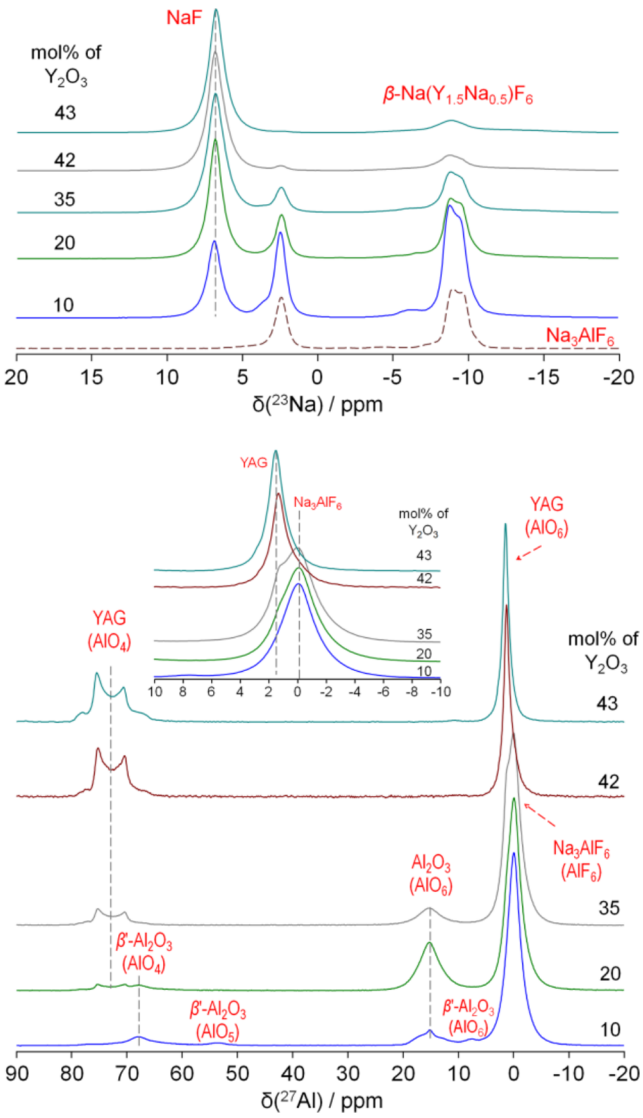

Figure 3. Solid-state ^{27}Al (lower part) and ^{23}Na (upper part) NMR spectra of the Na_3AlF_6−Y_2O_3 solidified samples after thermal analysis. The assignment of resonances was made based on the following references and reflections: YAG (^{27}Al),[24] β'-Al_2O_3 (^{27}Al).[25]

■ YAG SYNTHESIS EXPERIMENTS

Na_3AlF_6-Y_2O_3. The previous XRD and NMR analyses of the solidified samples after thermal analysis clearly showed that Na_3AlF_6−Y_2O_3 may be considered a very promising system for the low-temperature synthesis of YAG materials. To find out the most effective route for the YAG synthesis, several experiments with different reactant compositions, temperatures, and holding times were performed in a platinum crucible in an open-air furnace. The most effective route in this regard means the lowest synthesis temperature possible with the highest yield of YAG in the reaction mixture.

https://doi.org/10.1021/acs.cgd.4c00684
Cryst. Growth Des. 2024, 24, 7494−7503

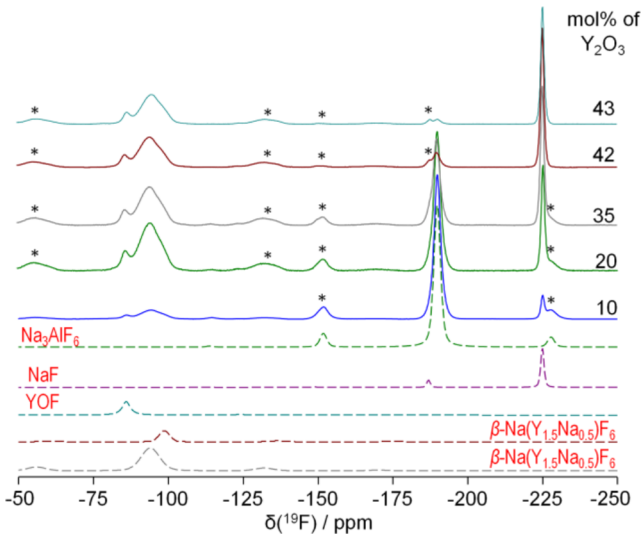

Figure 4. Solid-state ^{19}F NMR spectra of the Na_3AlF_6−Y_2O_3 solidified samples after thermal analysis. The assignment of resonances was made based on the following references and reflections: YOF,[26,27] β-Na($Y_{1.5}Na_{0.5}$)F_6;[28] *—spinning sidebands.

Figure S1 (in the Supporting Information) shows the coordinates of these synthesis experiments within the Na_3AlF_6−Y_2O_3 phase diagram. Based on these compositions, the synthesis experiments can be divided into three groups (4, 43, and 80 mol % of Y_2O_3). Based on the synthesis route, the samples can be divided into two groups: the liquid synthesis route and the solid/partly melted state synthesis. The visual observation of the reaction mixture after the synthesis experiments was able to clearly show whether the particular reaction mixture was fully melted during the holding time in the furnace.

Figures 5−7 show the results of the XRD analysis of the samples after synthesis experiments.

The samples from the synthesis using the fully liquid route show results that correlate very well to the results of the XRD analysis taken after the thermal analysis (Figure 2). The results of the sample after the synthesis with the lowest concentration of Y_2O_3 (4.8 mol %) contain the reflections of Na_3AlF_6, NaF, β-Na($Y_{1.5}Na_{0.5}$)F_6, and β-YOF (Figure 5). Moreover, a crystalline condensate was also found on the lid of the Pt crucible after this synthesis. The XRD analysis of the condensate subsequently showed the presence of $NaAl_5O_8$ (Na-β'-alumina) and Al_2O_3.

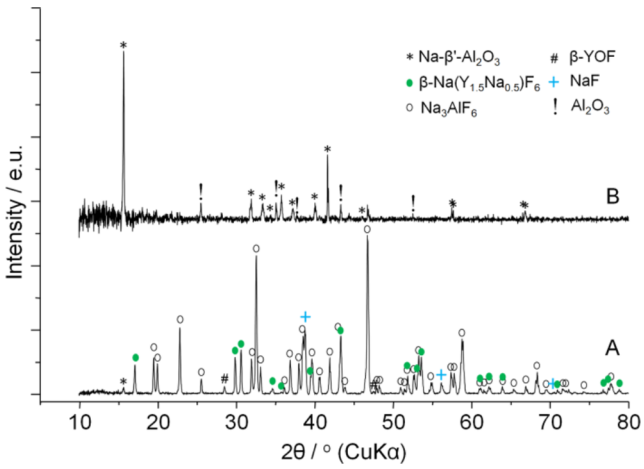

Figure 5. XRD patterns of the samples Na_3AlF_6−Y_2O_3 (4.8 mol % of Y_2O_3) melted at 1020 °C for 4 h. (A) XRD results of the sample itself; (B) XRD of the condensate found on the lid.

The results of the synthesis of the sample with coordinates 680 °C and 43 mol % of Y_2O_3 (eutectic composition) are depicted in Figure 6 (B_1 and B_2). The sample was like in the case of the thermal analysis, also separable into two different parts. The results from this liquid synthesis experiment also correlate with the XRD results obtained after the thermal analysis, although for the synthesis experiments, an open-air atmosphere was used. The patterns of the harder part (B_1) contain reflections of YAG, β-Na($Y_{1.5}Na_{0.5}$)F_6, and NaF. The softer part (B_2) contains only reflections of β-Na($Y_{1.5}Na_{0.5}$)F_6 and NaF and practically no reflections of YAG.

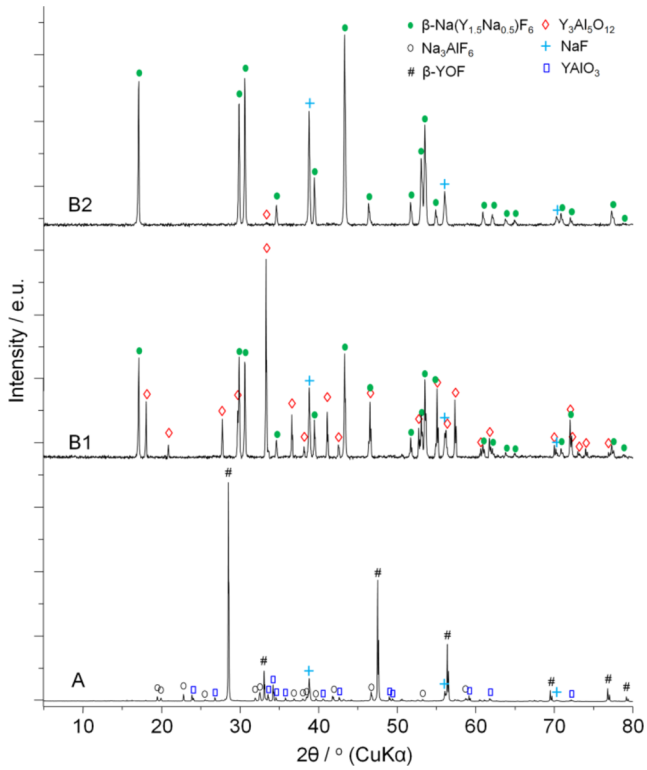

Figure 6. XRD patterns of the samples with 43 mol % Y_2O_3 synthesized at 600 °C (A) and at 680 °C (B_1—the harder part of the sample, B_2—the softer part of the sample). Time of the synthesis in both cases: 4 h in open-air atmosphere.

XRD analysis of the sample prepared in the solid state (below the eutectic temperature, Figure 6A) showed a different picture: a relatively strong reflection of β-YOF and then smaller reflections of $YAlO_3$, NaF, and Na_3AlF_6. $YAlO_3$ is yttrium aluminum oxide with a perovskite structure (YAP), known as an intermediary in the formation of YAG. Considering the results of both synthesis experiments with the eutectic composition (43 mol %), it appears that the temperature of 600 °C (solid-state route) is insufficient for the successful formation of YAG, so raising the temperature of the reaction mixture above the melting point appears to be critical for the formation of YAG.

In the sample with 80 mol % of Y_2O_3 in cryolite and synthesized at 750 °C, the XRD patterns contain NaF

https://doi.org/10.1021/acs.cgd.4c00684
Cryst. Growth Des. 2024, 24, 7494−7503

reflections (small intensity reflections), β-YOF (strong intensity reflections), and unreacted Y_2O_3 (strong intensity reflections) (Figure 7). Additionally, the same sample was

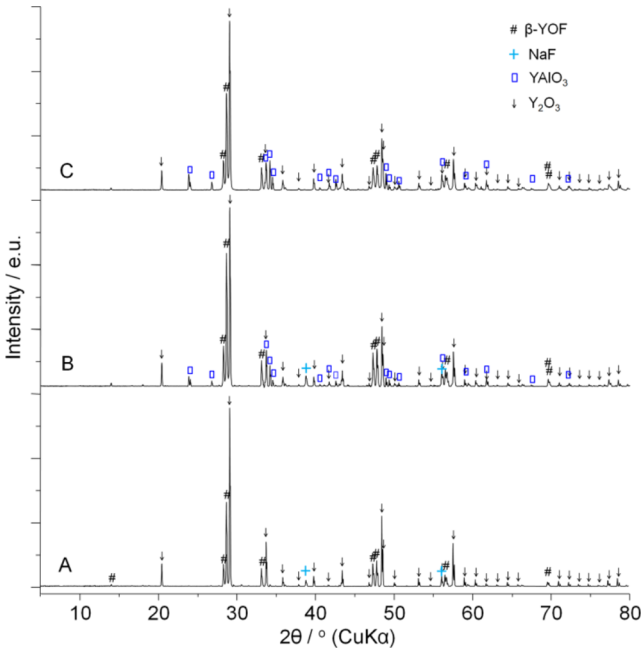

Figure 7. XRD patterns of the samples Na_3AlF_6−Y_2O_3 (80 mol % of Y_2O_3) melted at 750 °C (A), 1020 °C (B), and 1250 °C (C) during 4 h in open-air atmosphere.

heated even to 1020 °C (for 4 h) and analyzed. Its XRD pattern contains reflections of the same phases, NaF, β-YOF, and Y_2O_3. Besides that, the pattern contains a reflection of a new phase, $YAlO_3$. With a further increase in temperature to 1200 °C, the reflections of NaF in this sample disappeared, and the reflection intensities of $YAlO_3$ increased (Figure 7C).

Based on the latest results, it is possible to conclude that decreasing the Na_3AlF_6/Y_2O_3 ratio in the reaction mixture prevents YAG synthesis in favor of the synthesis of YAP.

YAG synthesis experiments were performed with different cryolite ratios (NaF/AlF_3).

To characterize the real potential of a whole molten NaF−AlF_3 system as a reaction medium for the preparation of YAG, in which molten cryolite represents only a tiny part, a series of synthesis experiments with different NaF/AlF_3 ratios has been performed (NaF−Y_2O_3, AlF_3−Y_2O_3, NaF−Na_3AlF_6−Y_2O_3, $Na_5Al_3F_{14}$−Y_2O_3). The phase diagram of the NaF−AlF_3 system (Figure S2) contains two eutectic points, E_1 (75 mol % NaF, t_{eut} = 888 °C) and E_2 (58 mol % NaF, t_{eut} = 695 °C) and two complex species: congruently melting cryolite (Na_3AlF_6, 75 mol % NaF, t_{mp} = 1011 °C) and incongruently melting chiolite ($Na_5Al_3F_{14}$, 62 mol %, t_{mp} = 738 °C).[21] From the parameters of both complex species and parameters of the eutectic points in the NaF−AlF_3 system, it is clear that there might still be some room, within the frame of the NaF−AlF_3 system, for decreasing the reaction temperature (e.g., using the eutectic composition and the eutectic temperature of the points E1 or E2 for the preparation of YAG, Figure S2). The analysis of the "boundary" reaction mixtures, NaF−Y_2O_3 and AlF_3−Y_2O_3, may, at the same time, help to elucidate and better understand the particular roles of NaF and AlF_3 during the preparation of YAG.

We performed a series of synthesis experiments with various NaF/AlF_3 ratios to assess the molten NaF/AlF_3 system as a reaction medium for YAG preparation. These experiments explored how different NaF/AlF_3 compositions influence YAG synthesis. The main findings of those experiments are listed below. More details of those experiments, including the XRD analysis, can be found in the Supporting Information (Figures S3−S6).

- NaF−Y_2O_3: In experiments conducted at 1020 °C with Y_2O_3 concentrations of 1 and 2 mol %, the low solubility of Y_2O_3 in molten NaF was evident, with β-YOF forming as the primary product, alongside NaF and unreacted Y_2O_3.
- NaF−Na_3AlF_6−Y_2O_3: Two experiments at 600 and 630 °C were performed to explore the possibility of reducing the YAG synthesis temperature. At 600 °C, β-YOF was the primary product, while at 630 °C, YAG and β-$Na(Y_{1.5}Na_{0.5})F_6$ were formed. This suggests that while NaF addition does not significantly lower the synthesis temperature, it plays a role in facilitating the formation of YAG.
- $Na_5Al_3F_{14}$−Y_2O_3: Chiolite was tested as a reaction medium at 860 °C. The results showed β-YOF, Na_3AlF_6, and Al_2O_3 as the main products, indicating that chiolite behaves differently than cryolite, likely due to the low solubility of Y_2O_3 in molten chiolite.
- AlF_3−Y_2O_3: An experiment was performed at 1000 °C without NaF, aimed to synthesize YAG using a solid-state reaction between AlF_3 and Y_2O_3. The products included YF_3, Al_2O_3, and $Y_5O_4F_7$, with no YAG formation. This highlights the importance of NaF in successful YAG synthesis, even at elevated temperatures.

ND: YAG SYNTHESIS EXPERIMENT

Na_3AlF_6−Y_2O_3−Nd_2O_3. To check the suitability of molten fluorides for the preparation of YAG-doped materials, an Nd:YAG synthesis experiment was performed with Na_3AlF_6, Y_2O_3, and Nd_2O_3. Yttrium aluminum garnet doped with neodymium (Nd:YAG) is the most well-known oxide crystal used as the active medium in solid-state lasers.[29,30] The Nd^{3+} dopant typically replaces a small percentage of the yttrium ions in the host crystal structure of YAG, and it is precisely the Nd ions that provide the leasing activity in the crystal. Molten cryolite can be used, based on the literature, as a good solvent for Nd_2O_3 (the eutectic concentration of the Na_3AlF_6−Nd_2O_3 system is around 12 mol %).[31] The other characteristics of the experiments were as follows; composition of the reaction mixture: Na_3AlF_6, Y_2O_3 (42 mol %), and Nd_2O_3 (7 mol %); temperature: 900 °C; duration: 4 h; atmosphere: open air. The powdered starting materials were all with purity greater than 99%.

In the YAG crystal structure, Y^{3+} ions inhabit dodecahedral positions, while Al^{3+} ions inhabit octahedral and tetrahedral positions. This arrangement results from variances in the ionic radii: O^{2-}(1.40 Å), Y^{3+}(1.02 Å), and Al^{3+}(0.51 Å).[32−35] Because the ionic radii of Y^{3+} ions and rare-earth ions are comparatively similar, trivalent ions of rare earth can substitute for Y^{3+} ions to a minor extent. The most common rare-earth ion used in this regard is Nd^{3+} (1.12 Å), with a doping molar concentration in YAG between 0.2 and 1.4%. Since the radius of the Nd^{3+} ion is bigger than the radius of Y^{3+}, it may be

https://doi.org/10.1021/acs.cgd.4c00684
Cryst. Growth Des. 2024, 24, 7494−7503

sometimes complicated to incorporate neodymium in the required amount into the yttrium sites of the crystal lattice.[33,36]

The Rietveld refinement of the XRD patterns of the solidified eutectic mixture of Na_3AlF_6 and Y_2O_3 with and without the addition of Nd_2O_3 are shown in Figures 8 and 9.

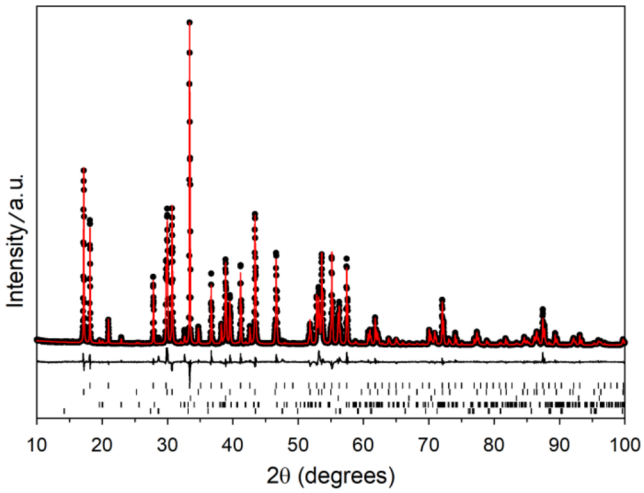

Figure 8. Rietveld refinement fit to the undoped sample (Na_3AlF_6 and 42 mol % Y_2O_3) synthesized at 900 °C for 4 h (open-air atmosphere). The black circles are data points, the red line is the fit, and the difference curve is beneath. The tick marks from top to bottom are the hkl positions for YAG, β-$Na_{1.5}Y_{1.5}F_6$, NaF, Na_3AlF_6, and YOF. R_{wp} = 9.06%.

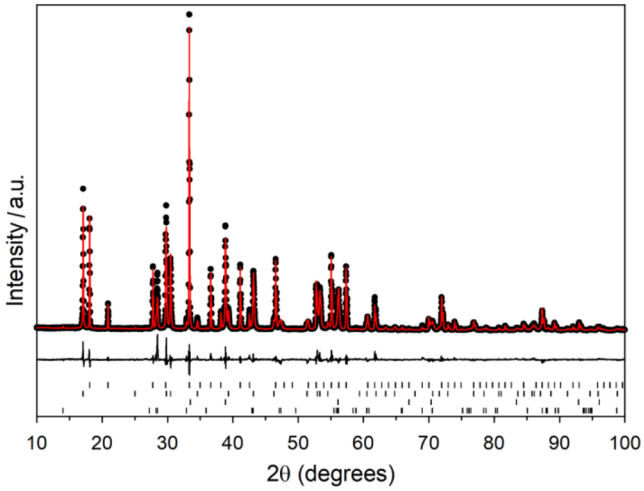

Figure 9. Rietveld refinement fit to the Nd-doped sample (Na_3AlF_6, Y_2O_3 (42 mol %), and Nd_2O_3 (7 mol %)), temperature: 900 °C, duration: 4 h, atmosphere: open air. The black circles are data points, the red line is the fit, and the difference curve is beneath. The tick marks from top to bottom are the hkl positions for YAG, $Na_{1.5}Y_{1.5}F_6$, NaF, and YOF. R_{wp} = 11.91%.

The undoped sample (Na_3AlF_6 and 42 mol % Y_2O_3) had the same parameters of the synthesis (900 °C, 4 h in an open-air atmosphere) as the Nd-doped sample. The final parameters of the refinement are given in Tables 1 and 2. The Rietveld refinement of the undoped sample had a R_{wp} of 9.06%. The R_{wp} of the fit of the doped sample was 11.91%. Both samples contain reflections of YAG as well as reflections of β-$Na(Y_{1.5}Na_{0.5})F_6$, NaF, and β-YOF. Small peaks of Na_3AlF_6 were also recorded in the undoped sample. No extra diffraction peaks were recorded in the sample with doped neodymium.

The peak position shifts to lower diffraction angles in the X-ray diffraction patterns are apparent as a result of the substitution of smaller Y^{3+} ions by larger Nd^{3+} ions in the host lattice (Nd:YAG has larger cell parameters than YAG). It needs to be stressed at this point that the 10% ionic radius difference between Y^{3+} and Nd^{3+} makes it relatively difficult to form highly doped Nd:YAG since solid solutions from the molten liquid usually only form if the difference of radii is smaller than 5%.[35]

The Nd^{3+} ions replace Y^{3+} in YAG without the need for charge adjustment. The increased size of the Nd^{3+} ions produces polyhedra with sides larger than those of Al^{3+} polyhedra. This affects the lattice, limiting the maximum feasible neodymium doping concentration to a few atomic weight percent.

The concentration of doped neodymium in our sample can be estimated to be around 0.32 wt % of Nd. This assessment is based on the comparison of the change of the cell parameter of YAG/Nd:YAG in our work (0.046%) and the work of Kostić et al. (0.116%).[33] The rest of Nd^{3+} was probably intercalated into the other compound present in our samples, β-$Na(Y_{1.5}Na_{0.5})F_6$. The reflection shifts of the XRD peaks of this compound toward lower angles (increase of the cell parameters) were also observed.

β-$Na(Y_{1.5}Na_{0.5})F_6$ compound is one of the two polymorphic forms of $NaYF_4$ known as hexagonal β-$NaYF_4$. The structure of that compound has three cation sites, one for Y^{3+} ions, one for both Y^{3+} and Na^+ ions, and the third for only Na^+ ions.[37] Previous research indicates that $NaYF_4$ is an excellent host lattice for various optically active lanthanide ions for upconversion luminescence applications (higher energy light emission upon lower energy excitation, e.g., emit visible light upon infrared excitation). The hexagonal β-form outperforms the cubic β-$NaYF_4$ for the luminescence of optically active lanthanide ions.[38,39] A wide variety of inorganic structures have been already proposed in the literature as matrices for lanthanide-based luminescent materials. Among the various potential inorganic host matrices, different fluoride substrates are being widely used due to their low phonon energy. According to the literature, β-$Na(Y_{1.5}Na_{0.5})F_6$ is a good multicolor luminescent matrix that can be doped with trivalent lanthanides to form the hexagonal $Na((Y_xLn_y)_{1.5}Na_{0.5})F_6$, where $x + y = 1$.[40−42]

■ CONCLUSIONS

In this work, we tried to use molten sodium cryolite (Na_3AlF_6) flux for low-temperature molten salt synthesis of YAG and Nd-doped YAG. The main idea behind that approach is based on the fact that molten fluorides, particularly sodium cryolite, are excellent solvents of oxides (Al_2O_3, SiO_2, La_2O_3, etc.). To the best of our knowledge, no papers have yet been published on the preparation of YAG materials (or any other functional oxides) utilizing the molten fluoride synthesis process.

For the low-temperature synthesis of YAG with the best yield, a molten Na_3AlF_6−Y_2O_3 reaction mixture has been used with the Y_2O_3 concentration of 43 mol %, which is approximately the eutectic composition of the system Na_3AlF_6−Y_2O_3. The other products were β-$Na(Y_{1.5}Na_{0.5})F_6$ and NaF. While β-$Na(Y_{1.5}Na_{0.5})F_6$ is also a valuable product (as a laser material), NaF can be easily washed away after synthesis from the reaction mixture with water. Rapid cooling

https://doi.org/10.1021/acs.cgd.4c00684
Cryst. Growth Des. 2024, 24, 7494−7503

Table 1. Final Parameters of Rietveld Refinement of Undoped Sample (Na_3AlF_6 and 42 mol % Y_2O_3) Prepared at 900 °C for 4 h in an Open-Air Atmosphere

	$Y_3Al_5O_{12}$	$Na_{1.5}Y_{1.5}F_6$	NaF	Na_3AlF_6	YOF
phase fraction/wt %	36.5(1)	37.1(1)	19.1(1)	7.0(1)	0.37(1)
a (Å)	12.00819(9)	5.9707(3)	4.63367(9)	5.4068(6)	3.8205(9)
b (Å)				5.5938(7)	
c (Å)		3.52901(5)		7.7685(8)	18.762(4)
β (deg)				90.16(1)	
V (Å^3)	1731.54(3)	108.952(6)	99.489(6)	234.96(3)	237.16(6)

Table 2. Final Parameters of Rietveld Refinement of Nd-Doped Sample (Na_3AlF_6, 42 mol % Y_2O_3, and 7 mol % Nd_2O_3) Prepared at 900 °C for 4 h in an Open-Air Atmosphere

	$Y_3Al_5O_{12}$	$Na_{1.5}Y_{1.5}F_6$	NaF	YOF
Phase fraction/wt %	36.7(1)	28.8(1)	30.5(2)	4.04(4)
a (Å)	12.01373(13)	5.9881(8)	4.63293(10)	3.8371(4)
c (Å)		3.5552(1)		18.943(2)
V (Å^3)	1733.94(5)	110.40(2)	99.377(3)	241.53(4)

of the reaction mixture ex-post synthesis may be, however, the way how to separate/prepare single-phase YAG material. Nonetheless, more experimental work is still needed in this regard to identify effective and selective solvents/methods.

The phase equilibria and phase diagram of the Na_3AlF_6–Y_2O_3 system have been measured prior to the synthesis experiments since there is so far no information in the literature about the phase equilibria in the Na_3AlF_6–Y_2O_3 system and solubility of Y_2O_3 in molten Na_3AlF_6. The thermal analysis within the investigated concentration range −45 mol % Y_2O_3 revealed that the Na_3AlF_6–Y_2O_3 system is probably a simple eutectic system with one inflection (22.0 mol % Y_2O_3, 920 °C) point and one eutectic point with the following coordinates: 43 mol % Y_2O_3, 620 °C.

The lowest temperature used in this work for the synthesis of YAG was 630 °C, and the holding time was 4 h in an open-air atmosphere. The synthesis in the solid state was, on the other hand, not successful in terms of the preparation of YAG. The solid-state synthesis in this regard means either to have the reaction temperature below the eutectic temperature of the Na_3AlF_6–Y_2O_3 system or the synthesis with a higher concentration of Y_2O_3 in the reaction mixture (beyond the eutectic concentration of Y_2O_3). The products in the solid-state synthesis were *β*-YOF, $YAlO_3$ (YAP, yttrium aluminum oxide with a perovskite structure), and unreacted Y_2O_3. The proper concentration ratio between Na_3AlF_6 and Y_2O_3, as well as a preparation temperature above the melting point (wet route), is both critical for the successful synthesis of YAG, as demonstrated by the results of all synthesis experiments.

It can be also concluded that the change in the cryolite ratio (NaF/AlF_3 ratio) in the reaction mixture from pure cryolite (1:3) toward higher concentrations of NaF did not substantially decrease the temperature of the synthesis of YAG. When we moved with cryolite ratio to the other side, toward AlF_3, using chiolite ($Na_5Al_3F_{14}$) and yttria for the synthesis in the liquid state (860 °C), only *β*-YOF, Na_3AlF_6, and Al_2O_3 were identified in the reaction mixture. When we used pure AlF_3 and yttria as reactants for the synthesis at 1000 °C (only solid-state reaction is possible in this system due to AlF_3 sublimation), the reaction mixture after synthesis contained YF_3, Al_2O_3, and $Y_5O_4F_7$.

When we reflect on doing these tests, the cryolite yttria systems with a composition around the eutectic point look finally like the best synthesis option (in terms of temperature and yield) for the synthesis of YAG materials.

For the low-temperature Nd:YAG synthesis, the molten Na_3AlF_6–Y_2O_3 reaction mixture with 7 mol % Nd_2O_3 has been used. The other products besides neodymium-doped YAG were in this experiment *β*-YOF, *β*-$Na(Y_{1.5}Na_{0.5})F_6$, and NaF. The incorporation of Nd into the YAG matrix increased the cell parameters (shifts to lower diffraction angles in the XRD patterns). Some Nd^{3+} ions were, however, intercalated also into the *β*-$Na(Y_{1.5}Na_{0.5})F_6$ matrix, making Nd:$Na(Y_{1.5}Na_{0.5})F_6$, which is, however, also a valuable functional material.

We believe that the low-temperature synthesis from the molten fluorides could be an interesting alternative to the already developed methods of the synthesis of different functional oxide materials. The main advantage of that approach is clear: an excellent solubility of different oxides and other compounds in fluoride melts, and a disadvantage, especially compared to chlorides, is the relatively low solubility of some fluorides in water to clean a final product after synthesis easily. Identifying the best reaction mixture(s) to prepare a single-phase YAG material (or other functional oxides/materials) and YAG materials doped with different dopants (e.g., Yb, Er, Ce, etc.) will be a matter of continuing future work.

■ ASSOCIATED CONTENT

Supporting Information

The Supporting Information is available free of charge at https://pubs.acs.org/doi/10.1021/acs.cgd.4c00684.

Phase diagrams with coordinates of the synthesis experiments. The details of the synthesis experiments with different cryolite ratios and XRD patterns from systems NaF–Y_2O_3, NaF–Na_3AlF_6–Y_2O_3, $Na_5Al_3F_{14}$–Y_2O_3, and AlF_3–Y_2O_3 (PDF)

■ AUTHOR INFORMATION

Corresponding Authors

Michal Korenko − *Institute of Inorganic Chemistry, Slovak Academy of Sciences, 845 36 Bratislava, Slovakia; CNRS, UPR3079 CEMHTI, 1D Av. de la Recherche Scientifique, 45071 Orléans, France; Loire Valley Institute for Advanced Studies, 45000 Orléans, France*; Phone: +421 2 59465 462; Email: uachmiko@savba.sk

https://doi.org/10.1021/acs.cgd.4c00684
Cryst. Growth Des. 2024, 24, 7494−7503

František Šimko − *Institute of Inorganic Chemistry, Slovak Academy of Sciences, 845 36 Bratislava, Slovakia; Centre of Excellence for Advanced Materials Application—CEMEA, Slovak Academy of Sciences, 845 11 Bratislava, Slovakia;* orcid.org/0000-0003-2390-1349; Phone: +421 2 59465 495; Email: uachsim@savba.sk

Authors

Mathieu Allix − *CNRS, UPR3079 CEMHTI, 1D Av. de la Recherche Scientifique, 45071 Orléans, France;* orcid.org/0000-0001-9317-1316

Aydar Rakhmatullin − *CNRS, UPR3079 CEMHTI, 1D Av. de la Recherche Scientifique, 45071 Orléans, France;* orcid.org/0000-0002-7328-5081

Michael J. Pitcher − *CNRS, UPR3079 CEMHTI, 1D Av. de la Recherche Scientifique, 45071 Orléans, France;* orcid.org/0000-0003-2044-6774

Graham King − *Material and Chemical Sciences, Canadian Light Source, Saskatoon, Saskatchewan, Canada S7N 2 V3;* orcid.org/0000-0003-1886-7254

Complete contact information is available at: https://pubs.acs.org/10.1021/acs.cgd.4c00684

Author Contributions

M.K., with M.A. and M.P., conceptualized and planned the project. M.K. and F.Š. prepared the samples. F.Š. did TA measurements. M.K. and F.Š did the synthesis experiments. A.R. carried out the NMR experiments and performed analysis of the NMR data. M.K., F. Š., M.A., and G.K. performed an analysis of the structural data. The manuscript was conceptualized and written by M.K. and by F.Š., with the contribution of all coauthors.

Notes

The authors declare no competing financial interest.

■ ACKNOWLEDGMENTS

The authors acknowledge support from the LE STUDIUM Loire Valley Institute for Advanced Studies in Orléans, France. The work was financially supported by the Slovak grant agencies APVV-19-0270, APVV-19-0461, and VEGA 2/0046/22. Financial support from the IR INFRANALYTICS FR2054 for conducting the research is also gratefully acknowledged. NMR measurements realized through the project: Pan-European Solid-State NMR Infrastructure for Chemistry-Enabling Access—PANACEA.

■ REFERENCES

(1) Ye, S.; Xiao, F.; Pan, Y. X.; Ma, Y. Y.; Zhang, Q. Y. Phosphors in phosphor-converted white light-emitting diodes: Recent advances in materials, techniques and properties. *Mater. Sci. Eng. R Rep.* **2010**, *71* (1), 1−34.

(2) Geusic, J. E.; Marcos, H. M.; Van Uitert, L. G. Laser oscillations in Nd-doped yttrium aluminum, yttrium gallium and gadolinium garnets. *Appl. Phys. Lett.* **1964**, *4* (10), 182−184.

(3) Nikl, M.; Yoshikawa, A. Recent R&D Trends in Inorganic Single-Crystal Scintillator Materials for Radiation Detection. *Adv. Opt. Mater.* **2015**, *3*, 463−483.

(4) Gan, L.; Zhi-Yong, M.; Fang-Fang, X.; Ying-Chun, Zh.; Xue-Jian, L. Molten salt synthesis of YAG:Ce^{3+} phosphors from oxide raw materials. *Ceram. Int.* **2014**, *40* (3), 5067−5071.

(5) Ikesue, A.; Kinoshita, T.; Kamata, K.; Yoshida, K. Fabrication and Optical Properties of High-Performance Polycrystalline Nd:YAG Ceramics for Solid-State Lasers. *J. Am. Ceram. Soc.* **1995**, *78*, 1033−1040.

(6) Jiao, H.; Ma, Q.; He, L. L.; Liu, Z.; Wu, Q. L. Low temperature synthesis of YAG:Ce phosphors by LiF assisted sol−gel combustion method. *Powder Technol.* **2010**, *198* (2), 229−232.

(7) Li, J. G.; Ikegami, T.; Lee, J.-H.; Mori, T.; Yajima, Y. Co-precipitation synthesis and sintering of yttrium aluminum garnet (YAG) powders: the effect of precipitant. *J. Eur. Ceram. Soc.* **2000**, *20* (14−15), 2395−2405.

(8) Cao, W.; Becerro, A. I.; Castaing, V.; Fang, X.; Florian, P.; Fayon, F.; Zanghi, D.; Veron, E.; Zandona, A.; Genevois, C.; Pitcher, M. J.; Allix, M. Highly Nonstoichiometric YAG Ceramics with Modified Luminescence Properties. *Adv. Funct. Mater.* **2023**, *33* (14), No. 2213418. April 4

(9) Cantarano, A.; Testemale, D.; Homeyer, E.; Okuno, H.; Potdevin, A.; Dujardin, Ch.; Ibanez, A.; Dantelle, G. Drastic Ce^{3+} Insertion Enhancement in YAG Garnet Nanocrystals Through a Solvothermal Route. *Front. Mater.* **2021**, *8*, No. 768087.

(10) Hoghooghi, B.; Healey, L.; Powell, S.; McKitrrick, J.; Sluzky, E.; Hesse, L. Synthesis of YAG:Cr phosphors by precipitation from aluminum and yttrium sulfate solutions. *Mater. Chem. Phys.* **1994**, *38* (2), 175−180.

(11) Mancic, L.; Marinkovic, K.; Marinkovic, B. A.; Dramicanin, M.; Milosevic, O. YAG:Ce^{3+} nanostructured particles obtained via spray pyrolysis of polymeric precursor solution. *J. Eur. Ceram. Soc.* **2010**, *30* (2), 577−582.

(12) Li, X.; Liu, H.; Wang, J.-Y.; Cui, H. M.; Han, F. YAG:Ce nano-sized phosphor particles prepared by a solvothermal method. *Mater. Res. Bull.* **2004**, *39* (12), 1923−1930.

(13) Bortolani, F.; Dorey, R. A. Molten salt synthesis of PZT powder for direct write inks. *J. Eur. Ceram. Soc.* **2010**, *30* (10), 2073−2079.

(14) Zhang, S. W.; Jayaseelan, D. D.; Bhattacharya, G.; Lee, W. E. Molten salt synthesis of magnesium aluminate ($MgAl_2O_4$) spinel powder. *J. Am. Ceram. Soc.* **2006**, *89* (5), 1724−1726.

(15) Yan, H.; Hu, Y.; Teng, X.; Long, Z.; Ye, H.; Zhuang, W. Influence of molten salt on luminescent intensity and particle size of Y_2O_3:Eu^{3+} phosphor. *J. Rare Earths* **2007**, *25* (6), 697−700.

(16) Trojan-Piegza, J.; Zych, E. Preparation of nanocrystalline Lu_2O_3:Eu phosphor via a molten salts route. *J. Alloys Compd.* **2004**, *380* (1−2), 118−122.

(17) Gupta, S. K.; Mao, Y. A review on Molten Salt Synthesis of Metal Oxide Nanomaterials: Status, Opportunity, and Challenge. *Prog. Mater. Sci.* **2021**, *117*, No. 100734.

(18) Yang, H.; Zhu, G.; Yuan, L.; Zhang, C.; Li, F.; Xu, H.; Yu, A. Characterization and luminescence properties of YAG:Ce^{3+} phosphors by molten salt synthesis. *J. Am. Ceram. Soc.* **2012**, *95* (1), 49−51.

(19) Wu, C.; Luo, A.; Du, G.; Qin, X.; Shi, W. Synthesis and luminescent properties of non-aggregated YAG:Ce^{3+} phosphors via the molten salt synthesis method. *Mater. Sci. Semicond. Process.* **2013**, *16* (3), 679−685.

(20) Grjotheim, K.; Kvande, H.; Qingfeng, L.; Zhuxian, Q. Metal Production by Molten Salt Electrolysis. In *Especially Aluminium and Magnesium*; China University of Mining and Technology Press: China, 1998.

(21) Thonstad, J.; Fellner, P.; Haarberg, G. M.; Híveš, J.; Kvande, H.; Sterten, A. Aluminium Electrolysis. In *Fundamentals of the Hall-Héroult Process*, 3rd ed.; Aluminium Verlag, 2001.

(22) Šimko, F.; Rakhmatullin, A.; King, G.; Allix, M.; Bessada, C.; Netriová, Z.; Krishnan, D.; Korenko, M. Cesium Oxo− Fluoro− Aluminates in the CsF−Al_2O_3 System: Synthesis and Structural Characterization. *Inorg. Chem.* **2023**, *62* (38), 15651−15663.

(23) Massiot, D.; Fayon, F.; Capron, M.; King, I.; Le Calve, S.; Alonso, B.; Durand, J. O.; Bujoli, B.; Gan, Z.; Hoatson, G. Modelling One and Two-Dimensional Solid-State NMR Spectra. *Magn. Reson. Chem.* **2002**, *40*, 70−76.

(24) Massiot, D.; Bessada, C.; Coutures, J. P.; Taulelle, F. A Quantitative Study of ^{27}Al MAS NMR in Crystalline YAG. *J. Magn. Reson.* **1990**, *90* (2), 231−242.

(25) Šimko, F.; Rakhmatullin, A.; Florian, P.; Kontrík, M.; Korenko, M.; Netriová, Z.; Danielik, V.; Bessada, C. (Oxo)(Fluoro)−

Aluminates in KF−Al_2O_3 System: Thermal Stability and Structural Correlation. *Inorg. Chem.* **2017**, *56* (21), 13349−13359.
(26) Scholz, G.; Dreger, M.; Bertram, R.; Kemnitz, E. Nanoscopic Yttrium Oxide Fluorides: Non−Aqueous Fluorolytic Sol−Gel Synthesis and Structural Insights by ^{19}F and ^{89}Y MAS NMR. *Dalton Trans.* **2015**, *44*, 13522−13529.
(27) Pan, H.; Gerstein, B. C.; Loeliger, H. R.; Vanderah, T. A. A Reexamination of ^{19}F NMR in Selected Solids, the Conductor Ag_2F and Reference Insulators for Studies of $YBa_2Cu_3O_7$-type Superconductors. *Appl. Magn. Reson.* **1990**, *1*, 101−112.
(28) Bessada, C.; Rakhmatullin, A.; Rollet, A. L.; Zanghi, D. High Temperature NMR Approach of Mixtures of Rare Earth and Alkali Fluorides: An Insight into the Local Structure. *J. Fluorine Chem.* **2009**, *130* (1), 45−52.
(29) Yadegari, M.; Asadian, M.; Saeedi, H.; Khodaei, Y.; Mirzaei, N. Formation of gaseous cavity defect during growth of Nd:YAG single crystals. *J. Cryst. Growth* **2013**, *367*, 57−61.
(30) Katsurayama, M.; Anzai, Y.; Sugiyama, A.; Kokie, M.; Kato, Y. Growth of neodymium doped $Y_3Al_5O_{12}$ single crystals by double crucible method. *J. Cryst. Growth* **2001**, *229*, 193−198.
(31) Berul, S. I.; Voskresenskaya, N. K.Reaction of CeO_2, Nd_2O_3, and Sm_2O_3 with molten fluorides *Zh. Neorg. Khim.* 1963; Vol. *8*, pp 1431−1434. (Russ.)
(32) Kolesov, R.; Xia, K.; Reuter, R.; Stöhr, R.; Zappe, A.; Meijer, V.; Hemmer, P. R.; Wrachtrup, J. Optical detection of a single rare-earth ion in a crystal. *Nat. Commun.* **2012**, *3*, No. 1029.
(33) Kostić, S.; Lazarević, Ž.Ž.; Radojević, V.; Milutinović, A.; Romčević, M.; Romčević, N.Ž.; Valčić, A. Study of structural and optical properties of YAG and Nd:YAG single crystals. *Mater. Res. Bull.* **2015**, *63*, 80−87.
(34) Peizhi, Y.; Peiyhen, D.; Yhiwen, Y.; Yulian, T. The growth defects in Czochralski-grown Yb:YAG crystal. *J. Cryst. Growth* **2000**, *218* (1), 87−92.
(35) Kanchanavaleerat, E.; Cochet-Muchy, D.; Kokta, M.; Stone-Sundberg, J.; et al. Crystal growth of high doped Nd:YAG. *Opt. Mater.* **2004**, *26* (4), 337−341.
(36) Zhang, M.; Guo, H.; Han, J.; Zhang, H.; Xu, Ch. Distribution of neodymium and properties of Nd:YAG crystal by horizontal directional solidification. *J. Cryst. Growth* **2012**, *340* (1), 130−134.
(37) Wang, F.; Chatterjee, D. K.; Li, Z. Q.; Zhang, Y.; Fan, X. P.; Wang, M. Q. Synthesis of polyethylenimine/$NaYF_4$ nanoparticles with upconversion fluorescence. *Nanotechnology* **2006**, *17* (23), 5786−5791.
(38) Krämer, K. W.; Biner, D.; Frei, G.; Gudel, H. U.; Hehlen, M. P.; Luthi, S. R. Hexagonal sodium yttrium fluoride based green and blue emitting upconversion phosphors. *Chem. Mater.* **2004**, *16*, 1244−1251.
(39) Heer, S.; Kampe, K.; Gudel, H. U.; Haase, M. Highly Efficient Multicolour upconversion emission in transparent colloids of lanthanide-doped $NaYF_4$ Nanocrystals. *Adv. Mater.* **2004**, *16*, 23−24.
(40) Escudero, A.; Becerro, A. I.; Carrillo-Carrión, C.; Núñez, N. O.; Zyuzin, M. V.; Laguna, M.; González-Mancebo, D.; Ocaña, M.; Parak, W. J. Rare earth based nanostructured materials: synthesis, functionalization, properties and bioimaging and biosensing applications. *Nanophotonics* **2017**, *6* (5), 881−921.
(41) Wang, L.; Li, Y. $Na(Y_{1.5}Na_{0.5})F_6$ Single-crystal nanorods as multicolor luminescent materials. *Nano Lett.* **2006**, *6* (8), 1645−1649.
(42) Guan, H.; Li, Y. $Na(Y_{1.5}Na_{0.5})F_6$:RE^{3+}(Dy^{3+}, Tb^{3+}, Eu^{3+}, Tm^{3+}, Ho^{3+}):Controllable morphology, multicolor light and thermal properties. *J. Alloys Compd.* **2021**, *859*, No. 157833.

https://doi.org/10.1021/acs.cgd.4c00684
Cryst. Growth Des. 2024, 24, 7494−7503